Available online at www.sciencedirect.com
ScienceDirect
International Journal of Heat and Fluid Flow 28 (2007) 653–664
International Journal of HEAT AND FLUID FLOW
www.elsevier.com/locate/ijhff

Flow in simplified and real models of intracranial aneurysms

György Paál [a,*], Ádám Ugron [a], István Szikora [b], Imre Bojtár [c]

[a] Department of Hydrodynamic Systems, Budapest University of Technology and Economics, P.O. Box 91, 1521 Budapest, Hungary
[b] National Institute of Neurosurgery, Budapest, Hungary
[c] Research Centre for Biomechanics, Budapest University of Technology and Economics, Hungary

Received 7 December 2006; received in revised form 27 February 2007; accepted 1 April 2007
Available online 22 May 2007

Abstract

Numerical flow simulations have been performed on simplified artificial intracranial aneurysm models, as well as on real models obtained from rotational digital subtraction angiography images. The simplified geometries provide a basic understanding of the flow and allow the study of the influence of certain geometrical parameters with high accuracy and controllability. The real aneurysm models demonstrate that there is an infinite variety of shapes and very complex flow patterns. Nevertheless, it is proposed in this paper that the aneurysms can be divided into four basic classes corresponding to typical flow patterns. Some features of these have been identified and associated with possible causes of growth and rupture.

Keywords: Intracranial aneurysm; Flow simulation; CFD; Hemodynamics

1. Introduction

Intracranial aneurysms are defined as thin-walled bulges of the arterial walls located on the basal surface of the brain. These lesions are found in approximately 5% of the population (The International Study of Unruptured Intracranial Aneurysm Investigators, 1999). Rupture of such aneurysms is the most frequent reason of subarachnoid hemorrhage, a special type of stroke that affects 0.1–0.15% of the population each year and results in death or permanent disability in 35–40% of its victims (Longstreth et al., 1985). The ethiology of intracranial aneurysms is not fully understood. Most aneurysms are thought to develop due to a combination of structural, physiological and hemodynamic factors. Similarly, little is known about the reasons of aneurysm rupture. Comparing the frequency of aneurysms (5%) with the yearly rate of subarachnoid hemorrhage (0.1–0.15%/year) it becomes evident that less than 1/3 of all aneurysms will ever rupture. Prevention of rupture can be achieved by either open skull surgery or by an intra-arterial approach. Surgical treatment requires isolation of the aneurysm and (in particular) its entry point, the ''neck''. The aneurysm is then excluded from the circulation by placing a metallic clip on the aneurysm neck (Mayberg et al., 1994). Alternatively, the arterial (endovascular) technique utilizes fine platinum coils to tightly pack the aneurysm's cavity and achieve blood stasis and subsequent aneurysm thrombosis (Guglielmi et al., 1991). Newly emerging methods aim to achieve this goal by modifying the blood flow within the parent artery and the aneurysm itself by placing a metallic endoprosthesis (stent) within the parent vessel across the entrance of the aneurysm (Szikora et al., 2006). Considering that all preventive techniques carry relatively high risk, it would be mandatory that only those lesions are treated that have a high likelihood of rupture and bleeding. Fig. 1 shows the typical locations of intracranial aneurysms. They often develop at branching points, or on the side wall of arteries, usually at the inward or outward curve of arterial bends.

* Corresponding author. Tel.: +36 1 463 2991; fax: +36 1 463 3091.
E-mail address: paal@vizgep.bme.hu (G. Paál).

0142-727X/$ - see front matter © 2007 Elsevier Inc. All rights reserved.
doi:10.1016/j.ijheatfluidflow.2007.04.004

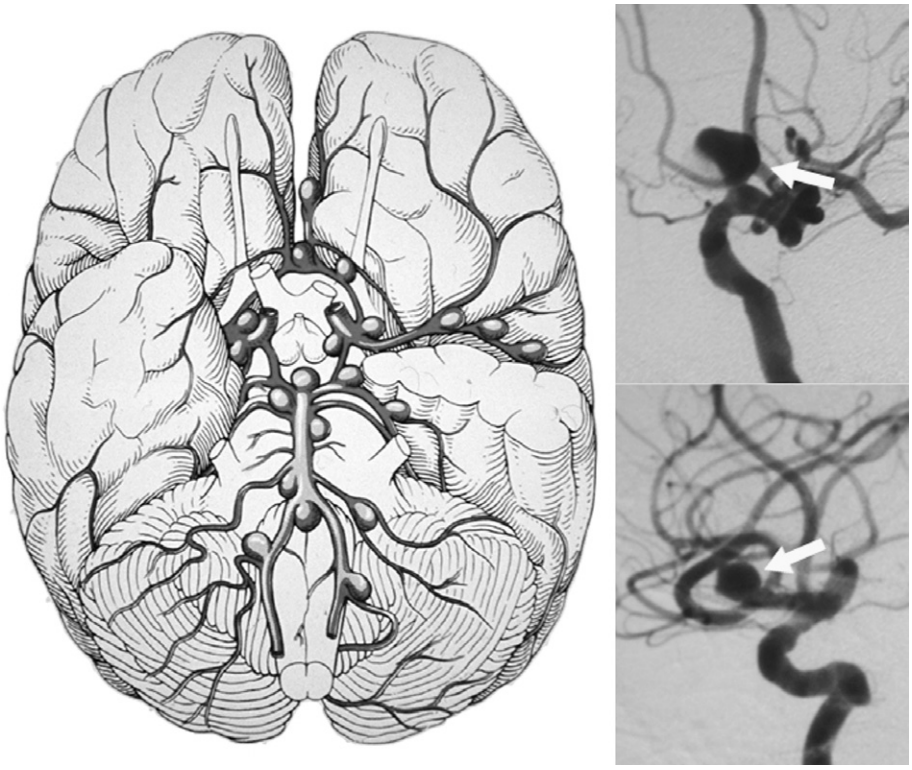

Fig. 1. Usual locations of appearance of intracranial aneurysms. Left: schematic illustration; right: angiographic images. (Courtesy of Prof. I. Nyáry, National Institute of Neurosurgery, Budapest.)

1.1. Purpose of this study

Hemodynamic stress at certain points of the arterial tree might be an important factor in both triggering aneurysm growth and leading to rupture of an existing aneurysm. Medical imaging techniques, such as digital subtraction angiography (DSA), computer tomographic angiography (CTA), or magnetic resonance angiography (MRA) are now capable of providing accurate three-dimensional information on intracranial vessel geometry. Current knowledge on the risk of bleeding from a known aneurysm (and subsequent decision on invasive treatment) is derived exclusively from such morphological information. As these techniques are not yet capable of delineating flow conditions within the visualized vascular segments, hemodynamic factors are not considered in the therapeutic decision-making process.

The purpose of this study is to develop a technique that is able to simulate arterial flow in and around intracranial aneurysms in order to study the effect of local hemodynamics on aneurysm growth and risk of aneurysm rupture. This information may lead to better indication of high risk surgical procedures.

1.2. Numerical simulations of aneurysm flows

There have been several research efforts to investigate the problem using numerical simulations. There are basically two approaches: using artificial models which are supposed to reflect the important geometrical and flow characteristics of the aneurysm and working on real models derived from medical imaging techniques. In the case of artificial models the researcher has complete freedom in preparing the geometry and the numerical mesh. Because of the relative simplicity, regularity and controllability of the geometry the mesh has usually a good quality. Examples for such artificial geometries are Egelhoff et al. (1999) (abdominal aneurysms), Shipkowitz et al. (2000) (abdominal aortic branches), Paál et al. (2004) (intracranial aneurysms). In the second approach the arterial geometry is obtained in a digital format consisting of voxels. It is possible to perform simulations on this mesh consisting of small cubes but these have a rough appearance since the surfaces of all cubes are in one of the three coordinate directions. In this case, especially near the wall, the results would be unrealistic. Various strategies have been applied to obtain a smoother mesh. One possibility is to deform and smooth the original hexagonal mesh (e.g. Shojima et al., 2004). It is also possible to redefine the surfaces in a smoother form using the original point set (Di Martino et al., 2001; Oshima, 2004; Hassan et al., 2004; Steinman et al., 2003). In this paper flow simulations in both artificial and real aneurysm geometries will be presented.

As mentioned above the factors leading to aneurysm growth and rupture are not clear. Many authors emphasize the potentially key role of the wall shear stress. However, there is considerable disagreement among researchers

whether the high or the low values, or the oscillation of shear (especially if associated with directional changes) are to blame. To the best knowledge of the authors, there is no convincing evidence supporting any of these hypotheses. Shojima et al. (2004) reported about 20 processed cases which all have more or less similar geometries. Out of these cases three have ruptured. They identified three groups of aneurysms, according to the locations of maximum shear stress. They tried to relate the aspect ratio of the sac with the wall shear stress but found only a very weak correlation. No significant correlation has been found between the magnitude of shear stress and the probability of rupture. Gonzalez et al. (1992) performed simulations on a sidewall aneurysm with curved parent vessel. They found that the flow pattern varies during the cycle with reverse flow in diastole near the aneurysm. Based on this they hypothesised a mechanism of aneurysm growth – namely that at the locations of largest shear stress oscillation the vessel wall is weakened and the aneurysm is prone to grow. Another idea is that the locally increased pressure due to a jet impinging on the aneurysm wall could be responsible for the growth. Hassan et al. (2004) simulated the flow in a giant vertebrobasilar aneurysm before and after therapeutic occlusion of one of the vertebral arteries. They detected an increased local pressure at the point of impingement of the jet on the aneurysm wall from the other vertebral artery. In the clinical follow-up it turned out that the aneurysm grew further exactly on this spot. This result looks encouraging; the question is what the relationship is between growth and rupture.

Another interesting question is to what extent the elasticity of the vessel walls plays a role in the flow in and around the aneurysms. Very few coupled (fluid–structure interaction = FSI) simulations have been performed. Di Martino et al. (2001) performed coupled fluid–structure interaction simulations for aortic aneurysms but conclude that their linearly elastic mechanical model contains too many uncertainties to make clinical decisions. Our research group performed some coupled simulations on simplified geometries which will not be shown here. Preliminary results indicate that the flow field is influenced only a very little by the elasticity of the wall so that the rigid wall approximation might be justified. However, further research is needed in this direction.

1.3. Experimental investigations of aneurysm flows

Similarly to the computational studies, there are two approaches to building flow models of aneurysms: simplified models and scaled-up real models extracted from angiography data. The models are usually made of transparent acrylic or Perspex blocks. Laser-based optical methods are almost exclusively used since the flow field is very complicated and the usage of intrusive probes would not only be cumbersome but would also disturb the flow while providing much less information. To avoid unwanted refractions at curved surfaces refractive index matching techniques are used. One of the central questions of these experiments is to determine to what extent the qualitative flow pattern changes during the cardiac cycle. The results are controversial and it is very likely that the answer is largely influenced by the exact shape of the unsteady input flow function. Liou and Liao (1997) investigated the flow field with particle tracking velocimetry (PTV) and by means of flow visualisation for varying curvature of the parent vessel and concluded that the intra-aneurysm velocities increase with increasing curvature. They also found that the qualitative appearance of the flow field is affected. Liou et al. (1997) measured velocity fields inside a model sidewall aneurysm using laser-Doppler velocimetry (LDV). They found slight variations in the inflow angle during the cycle but otherwise the flow field was similar. The peak shear stress was at the distal lip (as found in this paper) and the magnitude of the shear stress increased with decreasing sac size. Liou et al. (2004) used PTV and flow visualisation to study the unsteady flow pattern in an (artificial) model aneurysm with and without stents. It could be expected that the average flow velocity and the shear stresses are significantly reduced with the insertion of stents. However, they obtained a surprising result. In the unstented case the flow pattern remained unchanged throughout the cycle except for the velocity magnitude. Stent deployment across the neck of the aneurysm, however, produced qualitative changes of the flow pattern during the cycle. These changes were characteristic for the particular stent design. Tateshima et al. (2003) reported on LDV and particle image velocimetry (PIV) measurements in a real aneurysm model. Detailed time-resolved flow velocities were obtained and the variation of in- and outflow zones during the cycle identified. Benard et al. (2003) determined possible zones of very low shear stress caused by the insertion of a stent.

1.4. Artery wall properties

Healthy arteries are highly deformable complex structures, characterised by a nonlinear strain–stress curve with exponential rigidity in the higher strain ranges. This rigidity effect, characteristic for all biological tissues, is the result of rough collagen fibres which show typical anisotropic behaviour. Under normal circumstances the artery wall shows cylindrical orthotropy, generally accepted in the scientific literature. The material characteristics are either derived from in vivo experiments or from in vitro tests reflecting real conditions. Researchers would naturally prefer in vivo experiments; however, the data originating from physical reactions of the artery wall can only be measured by in vitro experiments at present. Under ex vivo conditions mechanical properties are subject to change due to biological degeneration, therefore arteries should be tested in a physiological saline solution properly oxygenated and at controlled temperature.

Mechanical properties of the aneurysm sac were analysed by Scott et al. (1972), Steiger et al. (1989) and Tóth et al. (1998). Tóth et al. (1998) measured the elasticity of

cerebral saccular aneurysms assuming spherical symmetry and homogenous elastic properties within the wall. They also considered the viscoelastic behaviour in the wall. Tóth et al. (2005) performed laboratory experiments, measuring the stress–strain functions of the arterial wall material using uniaxial and biaxial stretching tests. Human arterial strips were cut from both surgery and cadavers, from aneurysms and from normal arteries as control samples. The original location of the wall sample within the aneurysm was also taken into consideration in evaluating the measured results, to achieve precise description of the inhomogeneous and anisotropic nature of the material response. Longitudinal and circumferential, as well as thick (near to neck) and thin (near to the top – this is where rupture usually takes place) strips of human cerebral aneurysms were investigated.

The results show that the values of elastic modulus are *higher for women* in each case. The tensile strength of *thin strips* is higher in both circumferential and longitudinal direction than that of the thick ones but the difference between them is much larger in the circumferential than in the longitudinal direction.

In comparison with control human arteries the aneurysm samples experienced reduced elasticity in stretching at the beginning and the difference increased by further stretching. The aneurysm tissue reaches maximum extension relative to the control specimen at considerably smaller tensile strength.

1.5. Research strategy

We follow here a double research strategy. First, well-controlled, simple, artificial aneurysm models are investigated. This allows the generation of high-quality numerical meshes and carrying out highly accurate flow simulations. Then, further flow simulations are performed using real geometries obtained from DSA and an in-house mesh generation code. For both cases rigid wall geometry has been assumed. It turns out that the flow is significantly more complex in the real geometries than in the simplified ones. Also, because of the infinite variability of the shapes there are a number of different flow patterns even in similar geometries. Therefore, after examining a number of geometries, certain morphological classes are set up leading to flow pattern classes. The objective is to establish a correlation between flow pattern and aneurysm rupture risk. Another approach is to perform fully coupled flow–vessel wall deformation simulations (we shall present this work in a later publication). This way we can obtain additional information about wall stresses which might also be related to aneurysm growth and rupture.

2. Simulation details

2.1. The software

The ANSYS ICEM CFD commercial software was applied to generate the geometries of the artificial models and their computational meshes. The setup of the physical problem, the solution and the presentation and post-processing of the results was performed by various modules of ANSYS CFX. The tetrahedral meshes of the real artery geometries were created with an in-house code on the basis of the DSA data.

2.2. Geometries and meshes

Initially several simplified two-dimensional (2D) and three-dimensional (3D) geometries were made to study basic flow phenomena. Afterwards, real artery geometries were exported from rotational angiography images.

2.2.1. Artificial geometries

The traditional medical view of a sidewall aneurysm is depicted in Fig. 2. It consists of a straight pipe and a circular bulge sitting on it. The configuration is similar to a driven cavity and the ensuing flow pattern too. The reality, as indicated in Section 1, and as will be shown later, is more complex, and even relatively small deviations from the idealized geometry result in large changes in the flow pattern. Nevertheless it was found to be useful to perform a systematic study on the idealized geometries first before turning to the less regular shapes.

Four two-dimensional (2D) geometries were made with varying neck widths. The change in neck width was achieved by changing the parameter d ($d = 3$, 4, 4.54 and 5 mm).

The 2D geometry was a thin slice bordered by two planar surfaces. In the spanwise direction the geometry contained one computational cell since the solver is three-dimensional. Similarly, four three-dimensional (3D) geometries were created for studying the influence of the neck width on the flow pattern (Fig. 3).

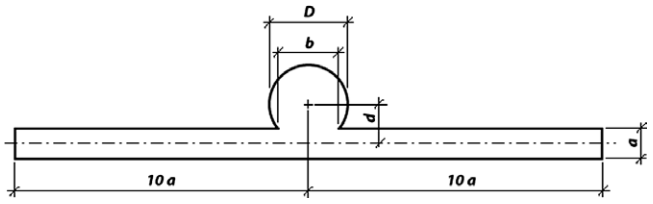

Fig. 2. The geometry of a simplified aneurysm containing the two main parts, the bulge and the pipe.

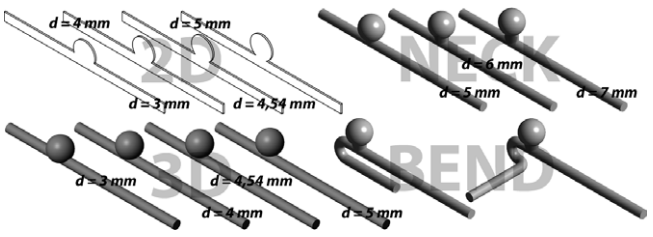

Fig. 3. Artificial models used for flow simulations. Top left: 2D models with varying neck width; bottom left: 3D models with varying neck width; top right: varying neck length; bottom right: bends before the aneurysm.

Another parameter which was varied is the neck length (contrary to the zero neck length so far). In the next step, based on careful observation of the real geometries, various types of bend were added on the parent vessel upstream of the aneurysm (Fig. 3).

The numerical meshes were topologically always identical: a block-structured hexagonal mesh was used in the pipe and in the aneurysm bulge (Fig. 4). This had an advantage over the unstructured mesh of a better computational accuracy and controllability, especially near the wall, in spite of the more cumbersome preparation of the mesh.

In the basic geometry, both in two and three-dimensions, very extensive mesh convergence studies were performed. In both cases five different meshes were tested and finally the mesh chosen contained 30,500 and 652,000 elements in 2D and 3D, respectively.

Also an unstructured mesh was tested in the same geometry without boundary layer mesh with a comparable number of elements. The idea behind this was that in the real geometries unstructured meshes would be used and we wanted to know its accuracy compared to the accuracy of the structured mesh. It turned out that the maximum relative error in velocity was around 10% and the largest values were detected in the boundary layer and in zones of low velocity. The error in the boundary layer is crucial because one of the interesting parameters is the wall shear stress.

2.2.2. Real geometries

The real geometries were obtained from rotational digital subtraction angiography (DSA). This technique takes 44 images with and 44 images without contrast material in the blood vessels, at various angles along a 180° semicircle around the patient's head. The contrast material is selected so that it strongly absorbs X-ray radiation unlike the surrounding tissues. The images are subtracted from each other and what remains is a three-dimensional digital image of the arterial system composed of 0.2 mm voxels. This image has to be further processed by expert MD-s who cut out the interesting artery section where the aneurysm is situated and where the flow ought to be simulated. Out of this uniform but rugged hexahedral mesh a smoother tetrahedral mesh is produced using an in-house code.

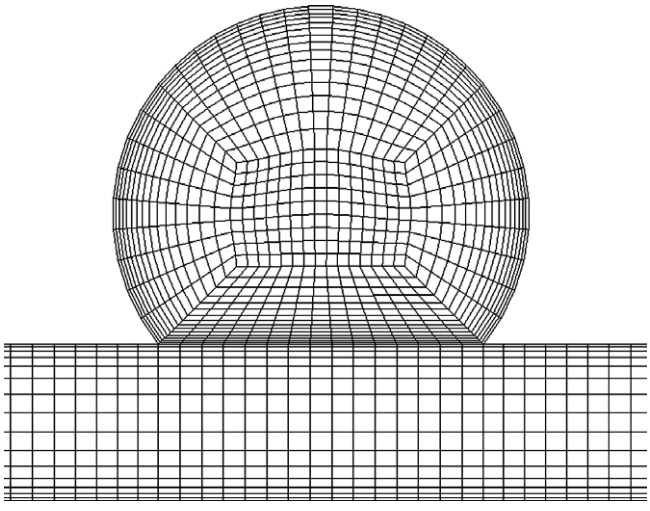

Fig. 4. Mesh topology used for the simplified geometries (in 3D this is the central plane).

2.3. Flow parameters, boundary conditions

The fluid investigated was assumed to be Newtonian, incompressible, with a density of 1050 kg/m^3, and a viscosity of 0.003 kg/m s. The flow was laminar, steady or unsteady.

The velocity boundary conditions at the walls of the geometries were assumed to be no-slip, impermeable and rigid. We performed coupled flow–wall elasticity simulations on simplified geometries and these showed that the influence of wall elasticity on the flow is small. In the 2D simulations symmetry boundary conditions were applied on the two planar faces. Both steady and unsteady cases were studied. In the stationary simulations a static inlet velocity with a parabolic profile, and a constant static pressure outlet were prescribed. In the unsteady simulations a time-dependent inlet velocity function was given (also with parabolic distribution in space). This is a synthetic function reproducing a typical shape of the cardiac cycle, shown in Fig. 5.

The outlet boundary condition remained constant pressure, modelling the fact that on the capillary level the pressure is really nearly constant (peripheral resistance). In principle the resistance of the whole arterial system between the studied arteries and the capillary level ought to be modelled. However, this resistance represents only an additive constant in the pressure level which has no importance in an incompressible flow with rigid walls and single outlet. With multiple outlets the difference between the outlet pressure levels and/or the resistances in the various artery branches will significantly influence the flow field. In the case of flexible walls, in addition, the absolute value of the pressure also becomes important because of the interaction with the wall stresses and deformations.

Both the spatial and temporal discretisation were second order. The relative residual level for convergence was 10^{-5}.

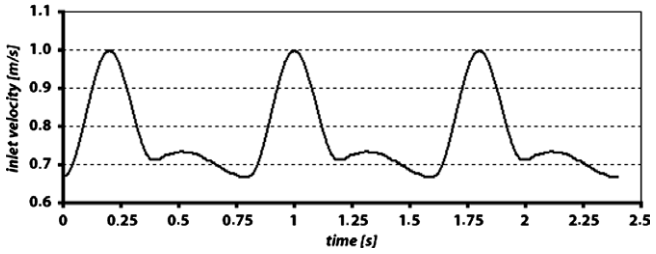

Fig. 5. Inlet velocity function.

3. Results for artificial geometries

3.1. Parametric studies in 2D

The purpose of the parametric studies in 2D was to quantify the effect of the neck width. First the velocity distribution is shown for a medium neck width ($d = 4$ mm) in Fig. 6. It is clear that the dominant motion is rotation with the highest velocity at the downstream (distal) end of the cavity. The inflow into the cavity takes place mainly also at the distal end whereas the outflow at the proximal end. Generally, however, there is little exchange of fluid between the main flow and the cavity flow. In Fig. 7. the distribution of the y velocity component (here: tangential) is shown. The x direction is the direction of the main flow, the y direction is perpendicular to it.

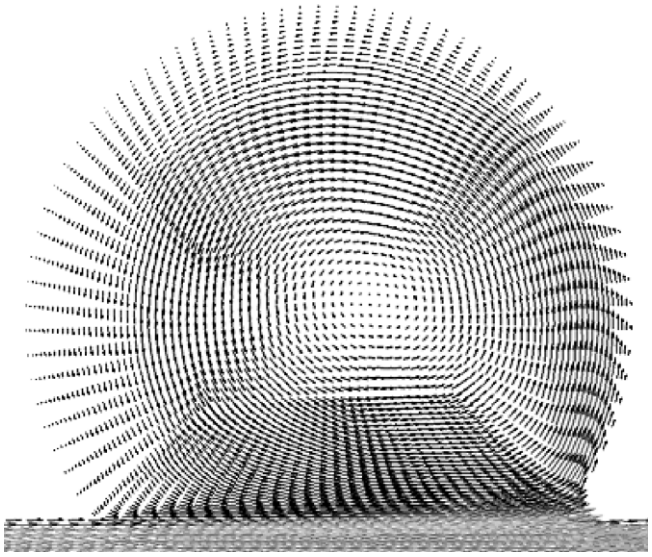

Fig. 6. Vector diagram of the vortex in the 2D aneurysm.

The distribution is not symmetrical. The velocity peak at the distal wall is about twice as high as at the proximal wall and the velocity gradient at the wall is also larger. There is a large region in the middle where solid body rotation takes place but there is no sign of potential vortex towards the edges. In order to characterize the "amount of rotating motion" in the aneurysm two parameters are introduced: the integral and the integral mean of the z component of the curl over the aneurysm. $\left(\mathrm{curl}(\vec{v})_z = \frac{\partial v_y}{\partial x} - \frac{\partial v_x}{\partial y}\right)$. The mean is necessary since the area of the cavity also changes by changing the neck width so that the various cases are otherwise not directly comparable with each other. Fig. 8a and b show these two quantities, respectively.

It can be seen, that the integral grows precisely linearly, whereas the average grows parabolically. Fig. 9 shows the distribution of shear stress along the wall starting before and ending after the aneurysm.

The distribution is qualitatively always the same with a sharp peak on the vessel wall immediately after the aneurysm. Within the aneurysm the shear stress is much lower than in the parent vessel. The value of maximum shear stress varies linearly with the neck width (not shown here).

When performing unsteady simulations within these geometries everything remains qualitatively the same, except that the concrete values of all the parameters vary in time according to the function in Fig. 5. The maximum shear stress occurs at the same place at every instant of the

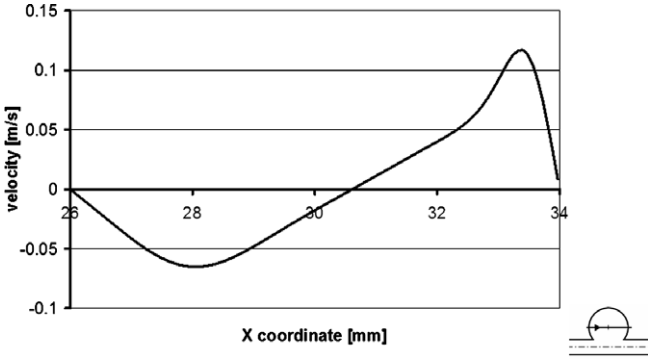

Fig. 7. Tangential velocity in the aneurysm along the horizontal diameter (see small figure bottom right).

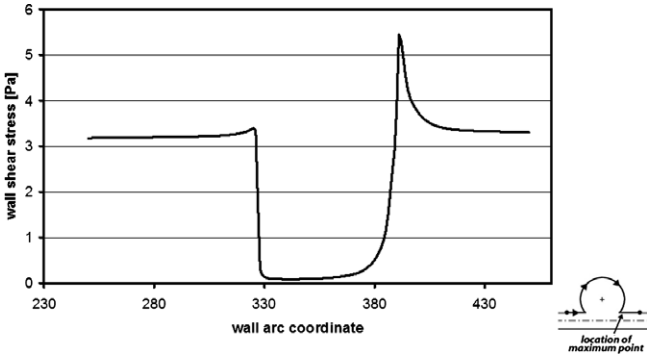

Fig. 9. The distribution of shear stress along the wall arc coordinate.

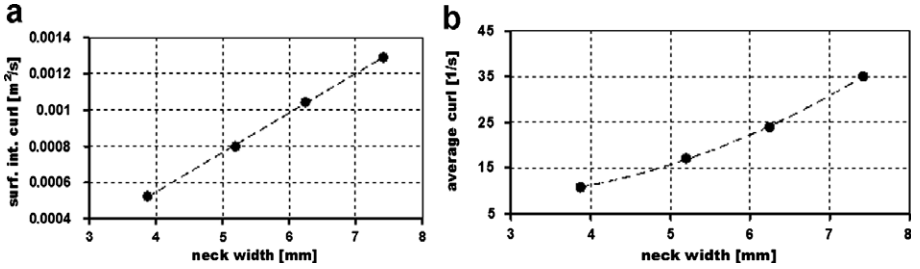

Fig. 8. Dependence of the surface integral (a) and surface average (b) of the curl in the aneurysm on the neck width in 2D.

cycle and the absolute maximum at the instant of the peak velocity.

3.2. Parametric studies in 3D

3.2.1. Influence of neck surface

First, similar parameter studies were performed as in 2D except that the independent variable here was the neck surface and the integral was evaluated over the whole volume. This is a surface produced by the intersection of a cylinder and a sphere. The functional dependences of both parameters on the neck surface were here monotonically increasing but degressive functions.

Observing the flow pattern in the perpendicular plane, it can be seen that the flow is symmetrical.

The maximum value of the shear stress appears again at the same place as in 2D (shown in Fig. 10): on the artery surface, shortly after the aneurysm. It is remarkable that the value of the maximum stress again depends linearly on the neck surface. The distribution along the length coordinate is very similar to the 2D case.

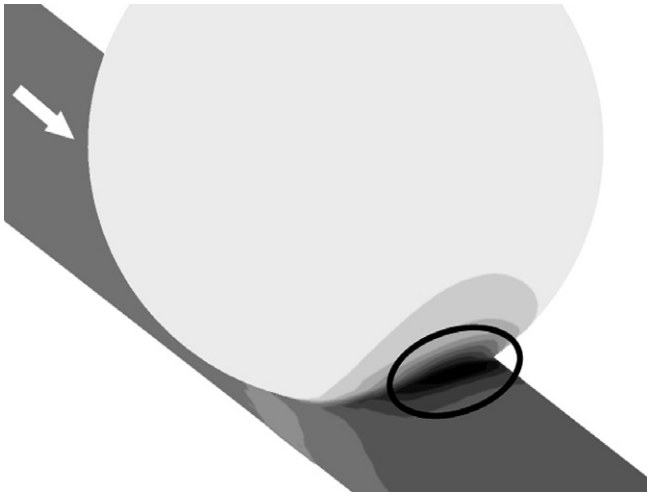

Fig. 10. Shear stress distribution near the aneurysm (the maximum is indicated with the ellipse).

3.2.2. Influence of neck length

The neck of finite length appearing in real aneurysms changes the flow conditions with respect to the case of neck with zero length. Three sizes were investigated; the distance d (distance of the centerline of the straight pipe and of the central point of the sphere) took values of 5, 6, 7 mm (Fig. 3, top right).

The single vortex which formerly filled the whole volume of the aneurysm breaks up into two separate vortices, indicated with dots or arrows in Fig. 11.

If the bend is built into the geometry in the way shown on the left hand side on the bottom right of Fig. 3, then the velocity increases on the outer side of the bend due to the secondary flow and the separation on the inner side. Thus the velocities within the aneurysm become larger and the shear stresses increase by several hundred percent. On the other hand, if the aneurysm is on the inner side of the bend then the velocities and shear stresses decrease relative to the straight artery case. In the case of two bends in perpendicular planes (right hand side of the bottom right of Fig. 3) the symmetry is broken, a complicated flow is created and the secondary flow is distorted. The velocities and the shear stresses are still much higher than in the straight case but somewhat lower than in the pure bend case. These two simple cases show that the aneurysms cannot be investigated in isolation; the flow before and after them have a vital importance. This is similar to the findings of Shipkowitz et al. (2000) who consider the influence of the inlet velocity profile on shear stresses in aortic branches. They found that the introduction of a tangential secondary flow profile decreases the maximum shear stress.

4. Results for real geometries

Having inspected and simulated a large number of real aneurysms we found that they have an infinite variety of morphologies. Yet, it was possible to establish typical groups among them. These are

(a) Aneurysm on the outer side of a bend;
(b) Aneurysm on the inner side of a bend;

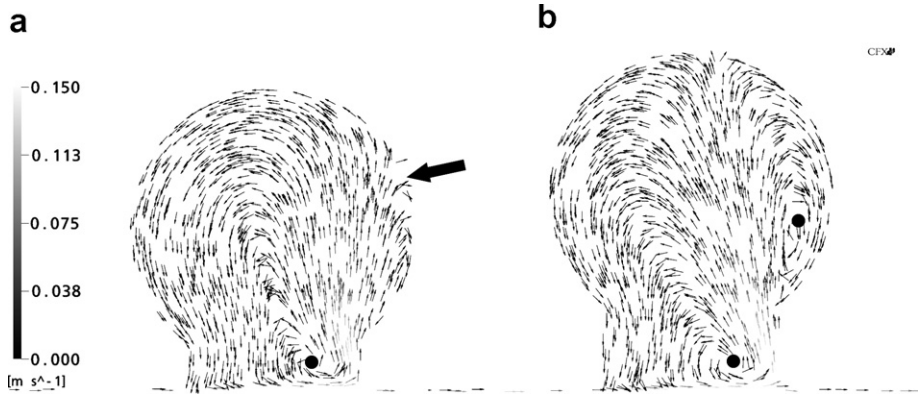

Fig. 11. Flow in the central plane of the aneurysm with nonzero neck length; (a) $d = 6$ mm; (b) $d = 7$ mm. The vortex centres are indicated with black dots or arrow.

(c) Bifurcating aneurysm;
(d) Atypical aneurysm.

One example of each case is presented in the form of the geometry, the wall shear stress distribution the pressure distribution and a picture demonstrating the flow. This latter picture is alternatively a vector diagram or a streamline diagram depending on which one seems to be more illustrative in the particular case. Although streamlines are difficult to interpret in an unsteady flow and the presentation of pathlines generated by hypothetical particles would be more correct, experience shows that in reality they differ from each other only very little. All the results are for the systole but other phases of the cardiac cycle are qualitatively similar.

4.1. Case (a): Aneurysm on the outer side of the bend

For this geometry, the shear stress, the pressure and the streamlines can be seen in Fig. 12. The aneurysm sac is located immediately distal to the bend. Just as in the case of the artificial models the maximum shear stress appears on the parent artery wall downstream of the aneurysm but the lower distal side of the aneurysm also displays a local maximum.

The pressure on the aneurysm wall is completely uniform; no distinguished places can be discovered. The flow in the parent artery proximal to the aneurysm gains a strong rotating component because of the double bend. It enters the sac much more directly than in the regular artificial geometry partly because of the secondary flow, partly because of the geometrical characteristics. The velocity in the aneurysm is therefore not negligible – the average is over 40% of the parent artery mean velocity as opposed to under 10% in the artificial geometries. As a further consequence, there is a distinct strong rotating motion within the aneurysm due to the asymmetry which is not present in the artificial geometries. The basic pattern is nevertheless not fundamentally different from the schematic pattern of the artificial case so that the flow enters the sac at the distal end and leaves at the proximal end of the neck.

4.2. Case (b): Aneurysm on the inner side of a bend

Although the size of the aneurysm is much larger than usual, this does not play an important role here. The flow within the aneurysm is extremely slow, and the direction appears random or chaotic (Fig. 13). This is a consequence of the reversed secondary flow in the parent artery relative to Case (a). The average velocity is of the same order of magnitude as in the artificial geometries, and this is a consequence of two opposing effects. On the one hand, the neck surface between parent artery and the sac is unusually large, which increases the momentum transfer. On the other hand, the sac is located on the ''unfavourable'' side of the bend in terms of secondary flow which decreases the momentum transfer. The pressure and the wall shear are completely homogeneous on the aneurysm wall and they display much lower values than both in Case (a) and in the artificial, straight artery case. Again, somewhat elevated values of shear stress appear on the distal side of the parent artery.

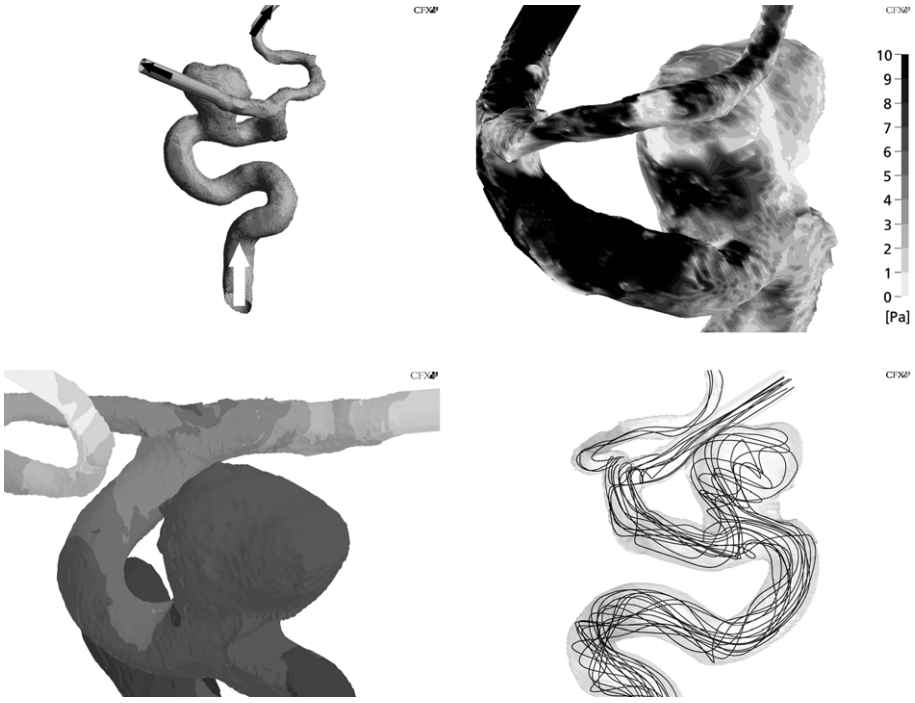

Fig. 12. Geometry, wall shear stress, wall pressure and streamlines for an example of Case (a).

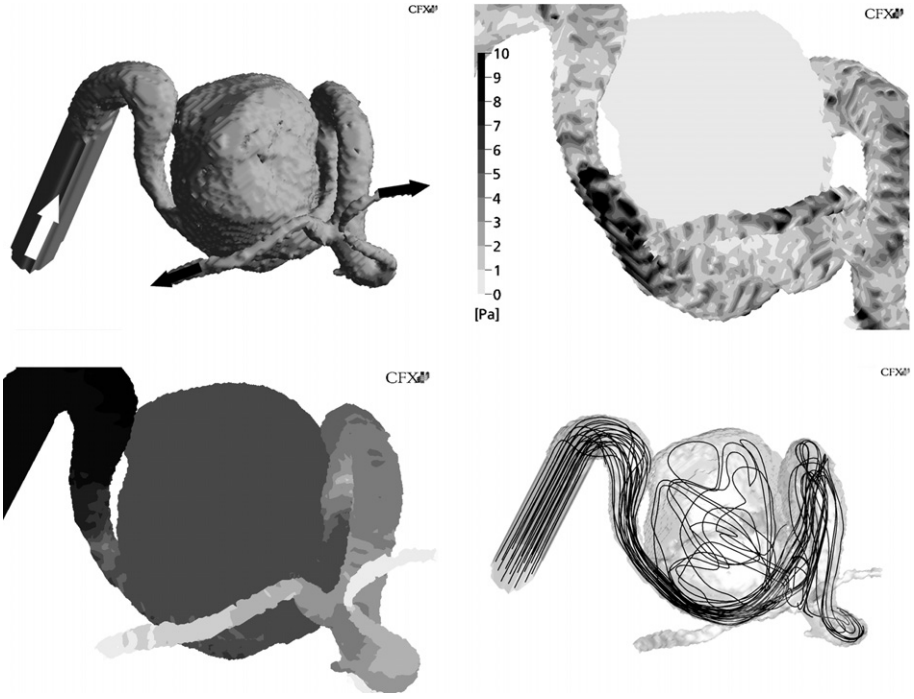

Fig. 13. Geometry, wall shear stress, wall pressure and streamlines for an example of Case (b).

4.3. Case (c): Bifurcating aneurysm

The flow in this case forms of a jet and impinges onto the opposite side of the aneurysm, indicated by an arrow. In the case presented in Fig. 14, the asymmetry makes the jet pass along the wall. At the impingement point of the jet there is a local maximum of the pressure and this appears consistently in all the similar geometries. In other cases (not shown here) the geometry is more symmetric and there the jet impinges onto the middle of the aneurysm wall, the flow divides into two branches along the wall and forms a double vortex. The fluid leaves then via the four smaller vessels; there is much more flow in the upper two than in the lower two branches. There is nothing

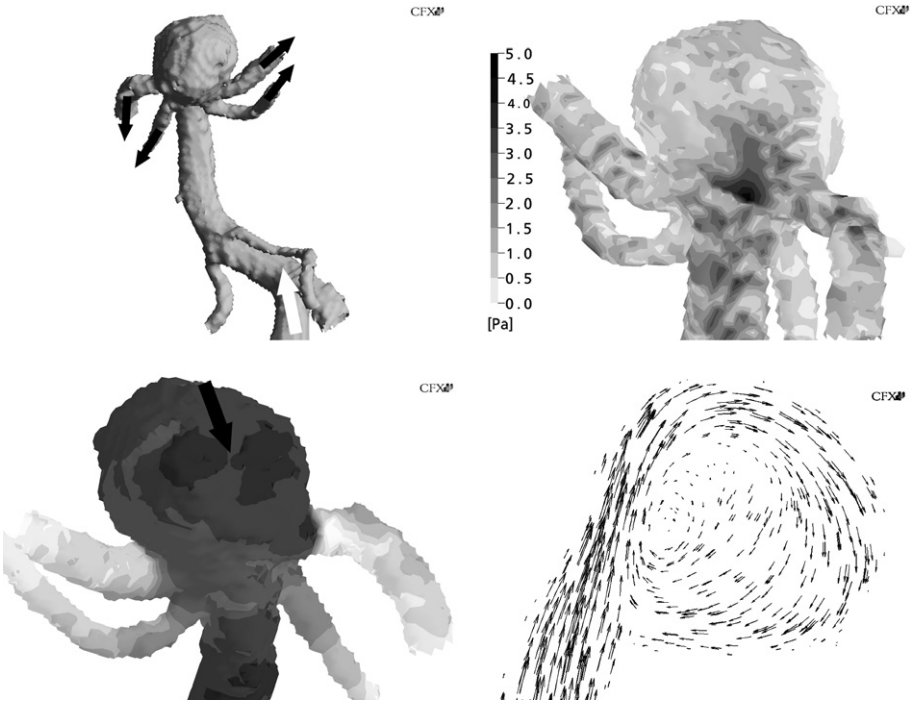

Fig. 14. Geometry, wall shear stress, wall pressure and vector diagram for an example of Case (c) (velocity vectors are scaled by size, the largest one is 0.7 m/s).

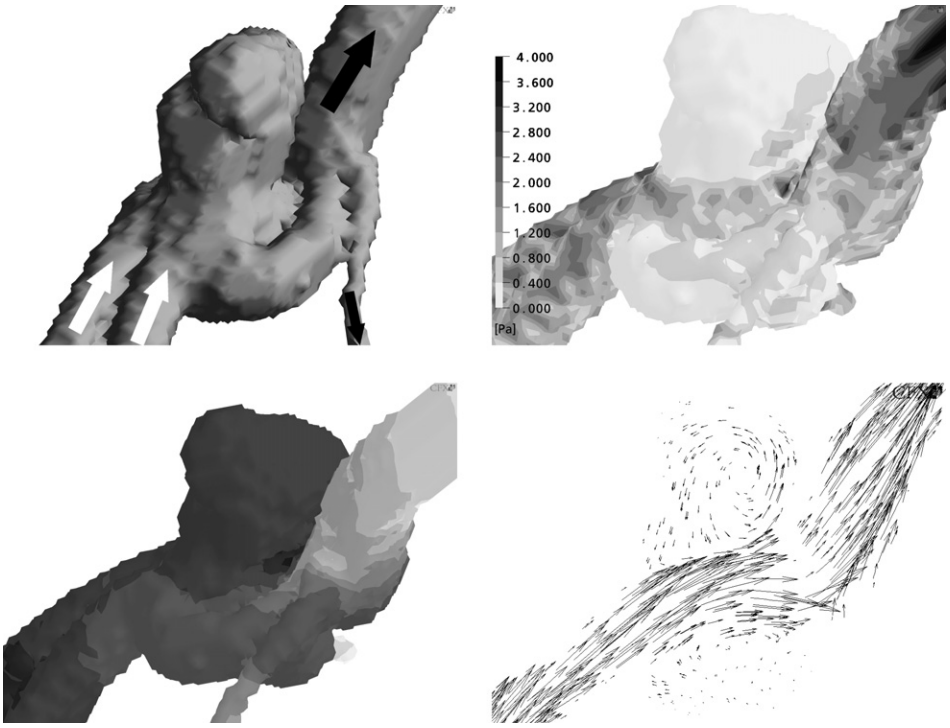

Fig. 15. Geometry, wall shear stress, wall pressure and vector diagram for an example of Case (d) (velocity vectors are scaled by size, the largest one is 0.5 m/s).

noteworthy about the shear stress distribution. The locally high pressure spot was noted also by Hassan et al. (2004) and they attributed the growth of the aneurysm to the local weakening of the tissue exactly at this spot.

4.4. Case (d): Atypical aneurysm

This geometry is a very rare case; a bilobulated aneurysm is generated at a location where the arteries join and immediately separate from each other to reunite again in a short distance (called a fenestration). The two lobes of the aneurysm are situated opposite to each other; on the dorsal and ventral side of the same artery. It is quite difficult to delineate the flow pattern and after careful inspection, it turns out that it is a double sidewall aneurysm with the usual homogeneous pressure distribution on the aneurysm wall and the low shear stresses. There is, however, some asymmetry in the system (Fig. 15) and therefore a jetlike high velocity flow reaches the neck of the upper aneurysm forming a stagnation point. Similarly to Case (c) there is a local high pressure spot there which might contribute to the further growth of the aneurysm.

5. Discussion

As mentioned in Section 1, there is no conclusive evidence concerning what physical processes contribute most to the growth and rupture of aneurysms. The four proposals put forward in the literature are (i) increased wall shear stress; (ii) reduced wall shear stress; (iii) high amplitude oscillation (possibly reversal of direction) of wall shear stress; and (iv) locally high pressure on the aneurysm wall. In this paper a crude classification of aneurysms was proposed and in a tentative way we can associate the various classes with the various parameters. Thus Case (a) can be associated with high shear stress, Case (b) with low shear stress, Case (c) with locally high pressure. The oscillatory shear stress depends more on the details of the geometry and of the unsteady boundary conditions, it needs more research. Our Case (d) may display any of the four particularities since its geometry is individual; it varies from case to case. The association of geometries with physical parameters should not be viewed as a strict one-to-one correspondence, rather a correlation. The geometries have a large variety and in individual cases another parameter might play a more important role in aneurysm growth and rupture than the one indicated here. Yet, geometry and related flow patterns might be used as potential guideline in estimating the natural history of an individual case. If follow-up studies can verify statistically significant correlation between the likelihood of rupture and the geometrical configuration of the aneurysm, then this would be not only medically significant information but would also shed some light on the cause of growth and rupture.

6. Conclusions

Numerical simulations have been performed for simplified and real models of intracranial aneurysms. The simulations on simplified models are more accurate because of the better quality mesh and they provide a basic understanding of the underlining flow pattern in typical aneurysm

geometries. It has been found that decreasing neck width reduces the amount of rotation in the aneurysm sac and increasing neck length has the same effect but in addition the structure of the flow changes. The flow in an aneurysm is influenced to a large extent by the velocity profile in the upstream artery. The secondary flow caused by various bends before the sac changes the flow pattern radically. The work on simplified aneurysms is very important and will be continued since it facilitates detailed systematic parametric studies aimed at examining the influence of boundary conditions and certain geometry changes on the flow pattern. In particular, it is interesting to identify the conditions that qualitatively change the flow pattern in and around the aneurysm during the cardiac cycle and those that result in reversal of flow and the direction of associated wall shear. Another direction of further work is the performance of coupled FSI simulations which has been started by our group. It is important to know to what extent the flow field itself is affected by the wall elasticity, and such simulations should provide information on mechanical loads on the wall which possibly contribute to aneurysm growth and rupture as well.

After evaluating several real aneurysms a classification scheme was presented here and for each class an example shown: the intracranial aneurysms were divided into four geometrical classes which correspond to four flow patterns associated with very different shear stress levels and velocity magnitudes. (With more research this scheme might be further refined.) It is proposed that in the long term evaluation of aneurysm ruptures the ''class'' be examined and if a significant correlation is found between rupture probability and a certain class that should have far-reaching therapeutic and theoretical consequences.

Numerical flow simulation is proving to be an effective tool for the better understanding of aneurysm flows and it is hoped that it will provide clinicians with a diagnostic tool of value for the decision-making processes when evaluating individual aneurysm cases.

Acknowledgement

This work was partially supported by the GE Hungary Rt. – Healthcare Division within the framework of the project ''Development of medical imaging solutions''. We sincerely appreciate the help of András Lassó. Partial support was provided by the Hungarian National Fund for Science and Research under grant Nr. OTKA T047150 OPR. Ádám Ugron wishes to thank for the support of his participation at the CMFF'06 by the SZEFH Foundation.

References

Benard, N., Coisne, D., Donal, E., Perrault, R., 2003. Experimental study of laminar blood flow through an artery treated by stent implantation: characterisation of intra-stent wall shear stress. Journal of Biomechanics 36, 991–998.

Di Martino, E.S., Guadagni, G., Fumero, A., Ballerini, G., Spirito, R., Biglioli, P., Redaelli, A., 2001. Fluid–structure interaction within realistic three-dimensional models of the aneurysmatic aorta as a guidance to assess the risk of rupture of the aneurysm. Medical Engineering & Physics 23, 647–655.

Egelhoff, C.J., Budwig, R.S., Elger, D.F., Khraishi, T.A., Johansen, K.H., 1999. Model studies of the flow in abdominal aortic aneurysms during resting and exercise conditions. Journal of Biomechanics 32, 1319–1329.

Gonzalez, G., Cho, Y.I., Ortega, H.V., Moret, J., 1992. Intracranial aneurysms: flow analysis of their origin and progression. American Journal of Neuroradiology 13, 181–188.

Guglielmi, G., Vinuela, F., Dion, J., Duckwiller, G., 1991. Electrothrombosis of saccular aneurysms via endovascular approach. Part 2: Preliminary clinical experience. Journal of Neurosurgery 75, 8–14.

Hassan, T., Ezura, M., Timofeev, E.V., Tomanaga, T., Saito, T., Takahashi, A., Takayama, K., Yoshimoto, T., 2004. Computational simulation of therapeutic parent artery occlusion to treat giant vertebrobasilar aneurysm. American Journal of Neuroradiology 25, 63–68.

Liou, T.-M., Liao, C.-C., 1997. Flowfields in lateral aneurysm models arising from parent vessels with different curvatures using PTV. Experiments in Fluids 23, 288–298.

Liou, T.-M., Chang, W.-C., Liao, C.-C., 1997. LDV measurements in lateral model aneurysms of various sizes. Experiments in Fluids 23, 317–334.

Liou, T.-M., Liou, S.-N., Chu, K.-L., 2004. Intra-aneurysmal flow with helix and mesh stent placement across side-wall aneurysm pore of a straight parent vessel. Journal of Biomechanical Engineering 126, 36–43.

Longstreth, W.T., Koepsell, T.D., Yerby, M.S., 1985. Risk factors for subarachnoid hemorrhage. Stroke 16, 377–385.

Mayberg, M.R., Batjer, H.H., Dacey, R., 1994. Guidelines for the management of aneurysmal subarachnoid hemorrhage. A statement for health care professionals form a special writing group of the stroke council, American Heart Association. Stroke 25, 2315–2328.

Oshima, M., 2004. A new approach to cerebral hemodynamics – patient-specific modelling and numerical simulation of blood flow and arterial wall interaction. IACM Expressions 16/04.

Paál, G., Bojtár, I., Szikora, I., 2004. Simulation of unsteady flow in brain aneurysms. In: First Hungarian Conference on Biomechanics, Budapest, 11–12 June.

Scott, S., Ferguson, G.G., Roach, M.R., 1972. Comparison of the elastic properties of human intracranial arteries and aneurysms. Canadian Journal of Physiology and Pharmacology 50, 328–332.

Shipkowitz, T., Rodgers, V.G.J., Frazin, L.J., Chandran, K.B., 2000. Numerical study on the effect of secondary flow in the human aorta on local shear stresses in abdominal aortic branches. Journal of Biomechanics 33, 717–728.

Shojima, M., Oshima, M., Tagaki, K., Torii, R., Hayakawa, M., Katada, K., Morita, A., Kirino, T., 2004. Magnitude and role of wall shear stress on cerebral aneurysm. Computational fluid dynamic study of 20 middle cerebral artery aneurysms. Stroke http://www.strokaha.org, doi:10.1161/01.STR.0000144648.89172.of.

Steiger, H.J., Asalid, R., Reulen, H.J., 1989. Growth of aneurysms can be understood as passive yield to blood pressure. Acta Neurochirurgy (Wien) 100, 74–78.

Steinman, D.A., Milner, J.S., Norley, C.J., Lownie, S.P., Holdsworth, D.W., 2003. Image-based computational simulation of flow dynamics in a giant intracranial aneurysm. AJNR American Journal of Neuroradiology 24, 559–566.

Szikora, I., Berentei, Z., Kulcsar, Z., Barath, K., Berez, A., Bose, A., Nyary, I., 2006. Endovascular treatment of intracranial aneurysms with parent vessel reconstruction using balloon and self expandable stents. Acta Neurochirurgica (Wien) 148, 711–725.

Tateshima, S., Vinuela, F., Villablanca, J.P., Murayama, Y., Morino, T., Nomura, K., Tanishita, K., 2003. Three dimensional blood flow analysis in a wide-necked internal carotid artery – ophthalmic artery aneurysm. Journal of Neurosurgery 99, 526–533.

The International Study of Unruptured Intracranial Aneurysm Investigators, 1999. Unruptured intracranial aneurysms – risk of rupture and risk of surgical intervention. The New England Journal of Medicine 339, 1725–1733.

Tóth, M., Nádasy, G., Nyáry, I., Kerényi, T., Orosz, M., Molnárka, G., Monos, E., 1998. Sterically inhomogeneous viscoelastic behavior of human saccular cerebral aneurysms. Journal of Vascular Research 35, 345–355.

Tóth, B.K., Raffai, G., Bojtár, I., 2005. Analysis of the mechanical parameters of human brain aneurysm. Acta Bioengineering and Biomechanics 7/1, 3–22.